Int. J. Electrochem. Sci., 10 **(2015)** 1742 - 1751

International Journal of
ELECTROCHEMICAL
SCIENCE
www.electrochemsci.org

Influence of Applied Potential on Wall-Bounded Water Flow

Arunas Pulmanas, Deivis Plausinaitis, Vytautas Daujotis[*]

Faculty of Chemistry, Vilnius University, 24 Naugarduko St, LT-03225 Vilnius, Lithuania
[*]E-mail: vytautas.daujotis@chf.vu.lt

Received: 14 November 2014 / *Accepted:* 22 December 2014 / *Published:* 30 December 2014

Measured potential dependences of flow velocities of aqueous hexafluorophosphate, perchlorate and chloride solutions bring to view velocity maxima, which are near the potentials of minima in earlier reported potential dependences of drag force. Earlier reported interfacial viscosity changes, calculated from drag force data, are is to some extent overestimated due to leaving out of account the interdependence of friction and pressure drags. The changes of interfacial layer properties, induced by applied potential, extend beyond the interface and result in the bulk effects such as the change of wall-bounded flow velocity.

Keywords: Water, Flow velocity, Applied potential, Drag force

1. INTRODUCTION

Piezoelectric resonator and drag force measurements have shown a decrease of interfacial viscosity of hexafluorophosphate, perchlorate and chloride aqueous solutions during polarization of gold electrode towards potential of zero charge [1, 2]. The shift in the potential of the viscosity minimum, obtained from drag force measurements, follows the shift in the potential of zero charge with a change in concentration according to the Esin-Markov relation. Tenfold increase in concentration of specifically adsorbing chloride shifts the potential of viscosity minimum by -46 mV, whereas tenfold increase in concentration of weakly adsorbing perchlorate results only in the negligible shift of the potential of viscosity minimum (-4 mV) [2].

Before discussing the potential benefits of wall-bounded liquid flow control by applying electrical potential to the wall, some answers should be obtained. In hexafluorophosphate and perchlorate solutions, thickness shear mode dual-piezoelectric resonator measurements of gold electrode have shown a minimum of interfacial viscosity, which ranges from 0.5 to 1% of the bulk viscosity, at the potential of zero charge. From drag force measurements, this minimum was obtained to be equal to approximately 5% of the bulk viscosity [1, 2]. It has been suggested that the empirical

equation, which has been used to calculate the changes of the viscosity at gold sphere electrode from drag force data, does not account for all effects when the electrode potential of the sphere is changed. Viscosity changes at gold sphere electrode have been calculated from the drag force data by assuming that the only reason of the drag force change with potential is the change in interfacial viscosity [1, 2]. First, the drag coefficients have been calculated from the measured force drag F_D values via equation [3]:

$$C_D = \frac{F_D}{(1/2)\rho u_\infty^2 A} \quad (1)$$

where ρ is a fluid density, A is a frontal area - the body as seen from the stream, which for a sphere of diameter d is $A = \pi(d/2)^2$ and u_∞ is an unbounded flow velocity, which has been obtained by correcting the measured average flow velocity for the wall effect [4].

An iterative procedure has been used to determine the unbounded flow velocity u_∞ as it appears in the drag coefficient expression (1), in Reynolds number, which for the sphere in a fluid of dynamic viscosity η is

$$\mathrm{Re} = \rho u_\infty d / \eta \quad (2)$$

and in their empirical relationship, which for the Reynolds number range from 1.5×10^3 to 1.2×10^4 is [4]

$$\lg C_D = 2.4751 + 2.5558w - 0.9295w^2 + 0.1049w^3 \quad (3)$$

where $w = \lg \mathrm{Re}$.

After determining u_∞, relationship (3) was used to calculate the change of Reynolds number from C_D change with potential. Then viscosity change with potential was calculated via Eq. (2). In this calculation, an attribution of the drag force change with potential only to the change of interfacial viscosity is an approximation. As a first approach it can be justified because there is no theory for sphere drag except creeping flow. The drag forces on a sphere come primarily from viscous shearing stresses (skin friction) and differences in pressure. Thereby, the drag force F_D on a sphere could be divided into two components, namely, frictional drag F_{Df} and pressure drag F_{Dp}. The effect of viscosity on frictional drag should be most pronounced. However, frictional drag and pressure drag are interdependent [3, 4]. The problem could be solved by measuring and analysing these drag components separately [5]. However, it is not possible for the purposes of present work due to insufficient accuracy of such measurements.

The purpose of present work is: to evaluate the possible change of wall-bounded solution flow velocity with electric potential of the wall; to explain why interfacial viscosity changes, calculated from the drag force data, are larger than those obtained from the piezoelectric resonator measurements; to discuss the potentiality of the use of wall electric polarization as a flow stability modifier for wall-bounded water flow.

2. EXPERIMENTAL

The experimental set-up for measurement of electrode potential effect upon the drag force on gold coated bearing ball and the flow velocity is the same as earlier (Fig. 1) [6].

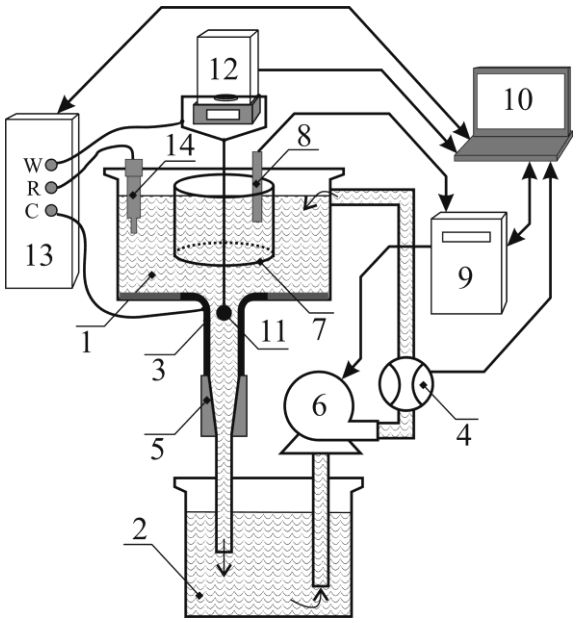

Figure 1. Schematic diagram of the solution flow system for measurement of electrode potential effect upon the drag force on gold coated bearing ball: 1 - upper reservoir, 2 - lower reservoir, 3 - bronze tube also used as counter electrode, 4 - flow volume meter, 5 – conical nozzle, 6 - stilling chamber, 7 - centrifugal pump, 8 - differential pressure transmitter, 9 - motion control tool, 10 – PC, 11 - gold coated bearing ball (working electrode), 12 - analytical balance, 13 – potentiostat, 14 - reference electrode. [6].

The set-up consists of upper reservoir (diameter $D_{reservoir} = 50\,\text{cm}$ and 40 l volume) (1 in Fig. 1) and lower reservoir (10 l volume) (2 in Fig. 1) joined by vertically positioned bronze tube (inner diameter $D_{tube} = 4.3\,\text{cm}$ and 40 cm long) (3 in Fig. 1). In order to decrease an additional flow friction induced by the sudden contraction of the flow entering the tube, the inlet of the bronze tube was rounded ($r_{rounding} = 0.23 D_{tube}$).

The velocity of the solution flowing through the tube was measured by flow volume meter (ETK-M with pulser, Zenner) (4 in Fig. 1), which detects time for each solution litre passed. The flow volume meter was modified by attaching laser and light detector in order to measure the frequency of light reflection from the whirligig blades. That allowed detecting time for each 25 ml of liquid passed in addition to detecting time for each solution litre passed. Flow velocity was controlled by changeable nozzles (5) mounted on the outlet of the bronze tube. The nozzles were made of polyamide with conical (the angle of the side was 86^{o}) holes narrowing from 4.3 cm to the diameter assuring the flow velocity needed. During the measurements centrifugal pump (6) was pumping solution from the lower reservoir back to the upper one. To decrease the upper solution surface undulation, the upper reservoir is replenished through six inlets located equidistantly and at the same height around the upper edge of the reservoir (only one inlet is shown in Fig. 1). In addition, a piece of tube (20 cm diameter) (7 in Fig. 1) is partially immersed into solution centre and serves as stilling chamber. The height of the solution level in the upper reservoir was controlled by differential pressure transmitter (DPTM500, Honeywell) (8 in Fig. 1) with an accuracy 1 mm. The overall solution flow was controlled by motion control tool (MST-10, Danfoss) (9 in Fig. 1) and computer (10), which according to the differential pressure

transmitter's readings monitored centrifugal pump operation by frequency converter in order to keep the preset height of solution level in the upper reservoir. Water flow system was not thermostated. When centrifugal pump has been pumping room temperature solution with an average flow velocity 0.16 m/s in the tube, the temperature of flowing solution has been steadily increasing by about 0.14^0C in an hour.

Bearing balls (9.52 mm diameter) made of steel were electrochemically coated with thin copper underlayer and gold (0.01 mm thick). Ball (11 in Fig. 3) was joined with gold wire (0.1 mm diameter) by arc welding using the charged capacitor as an electrical power supply. The gold wire served two-fold purpose. First, to hang the immersed ball on the weighing hook of the analytical balance (0.1 mg resolution) (12 in Fig. 1) located above the upper reservoir for drag force measurement. Second, to join the ball (working electrode) to the potentiostat (Reference 600 Potentiostat/Galvanostat/ZRA, Gamry) (13). The vertical bronze tube (4) was used as counter electrode. It should be noted that in all experiments the electrode potential of gold coated ball was changed into positive direction from the open circuitry potential. Thus, the inner surface of the bronze tube remained intact as it met only negative polarisation. Silver/silver chloride/(saturated KCl) electrode (14) was used as a reference electrode. Salt-bridge junction, filled with saturated NaCl solution, was used for measurements in sodium perchlorate solutions.

The hanged ball was located in the centre of the bronze tube and 1.5 cm below the upper reservoir bottom where nearly inviscid upstream flow converges and enters the tube. In this work, the average flow velocity was from 0.16 to 0.17 m/s for all drag force measurements. Then the Reynolds number for water flow at 20^oC through a 4.3-cm-diameter tube is $\mathrm{Re}_D = \rho u D_{tube} / \eta \approx 7000$. This means that flow should be fully turbulent. Actually, the turbulence develops gradually in the entrance of duct flow. Entering the tube the flow is nearly inviscid. Viscous boundary layers grow downstream, retarding the axial flow at the wall and thereby accelerating the centre-core flow. Fully turbulent flow develops at a distance from the entrance $L_e \approx 4.4\mathrm{Re}_D^{1/6} D_{tube}$ [3] what in our case yields $L_e \approx 82$ cm. Assuming linear growth of the thickness of viscous boundary layer with the distance from the entrance, one obtains that in the entrance region along the axis of the tube from 0 to 2 cm the wall boundary layers are less than 0.5 mm thick. That leaves 4.2 cm of inviscid core suitable for measurement of drag force on a sphere. These measurements and analysis of recorded drag force data are presented elsewhere [1, 2].

Even under invariable experimental conditions the obtained flow velocity data were scattered from their mean value up to 3%. This is not surprising because at moderate and higher Reynolds numbers the flow past immersed sphere creates pulsating wake in the rear of a sphere what results in fluctuation both of the flow velocity and of the drag force on a sphere. However, such scatter can make the change of the flow velocity with potential hardly noticeable. In addition, at present it is not possible to specify a global function of any form to fit a model to the data. For this reason, flow velocity dependences on the potential were recorded at potential sweep rates 0.5 mV/s. That allows to record large sets of densely sampled velocity and drag force data (5 drag force and 5 velocity values per second). To reveal possible dependence of flow velocity on the potential, the non-parametric regression analysis of these data was applied as it was done in an analysis of drag force data [1, 2]. The

LOESS procedure (local smoothing technique with tri-cube weighting and polynomial regression) was used to smooth the flow velocity data as a function of the potential.

0.01 M solutions of sodium hexafluorophosphate (98%, Sigma–Aldrich), sodium perchlorate (99,99%, Sigma-Aldrich) and sodium chloride (99%, Alfa Aesar), prepared in distilled water, were used. Solution was poured into the reservoirs and circulated for three hours before the measurements in order to ensure a steady temperature and flow regime during the measurement of the drag force dependence on potential.

3. RESULTS AND DISCUSSION

3.1. Electrode potential effect on the flow velocity during polarisation of gold coated sphere in hexafluorophosphate, perchlorate and chloride solutions

Measurements of the flow velocity during polarisation of gold coated sphere in hexafluorophosphate solution were performed in the potential region from −50 to +550 mV by detecting time needed for one flow litre to pass. Then the flow velocities in the bronze tube of 4.3 cm inner diameter (3 in Fig. 1) have been calculated and their LOESS fit vs potential of gold coated sphere is shown in Fig. 2A, solid line. The sampling proportion was chosen to be 0.4 since this produced a good tradeoff between noisy undersmoothing and oversmoothing which misses some of the peak-and-valley details in the data.

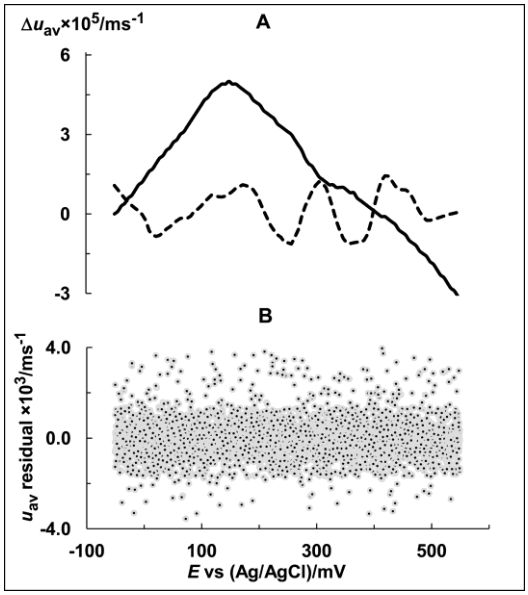

Figure 2. (A) LOESS fit (solid line, sampling proportion and polynomial degree equal to 0.4 and 1, respectively) for change of average velocity of flow past gold coated sphere vs potential of sphere in 0.01 M $NaPF_6$ aqueous solution and LOESS fit (dashed line, sampling proportion and polynomial degree equal to 0.2 and 1, respectively) for residuals of average flow velocity, $u_{av}^{E=-50\,\mathrm{mV}} = 0.15900$ m/s, six potential cycles at dE/dt=0.4 mV/s, (4157 flow velocity values), temperature from 21.9 to 22.6^{o}C; (B) Scatter plot of flow velocity residuals of LOESS fit (A, solid line) vs potential.

Flow velocity residuals of this LOESS fit (Fig. 2A) are scattered up to 3% (Fig. 2B) from the average flow velocity value (0.15900 m/s). In section 2, it has been mentioned that such scatter is unavoidable because at moderate and higher Reynolds numbers the flow past immersed sphere creates pulsating wake in the rear of a sphere. That results in fluctuation both of the flow velocity and of the drag force on a sphere.

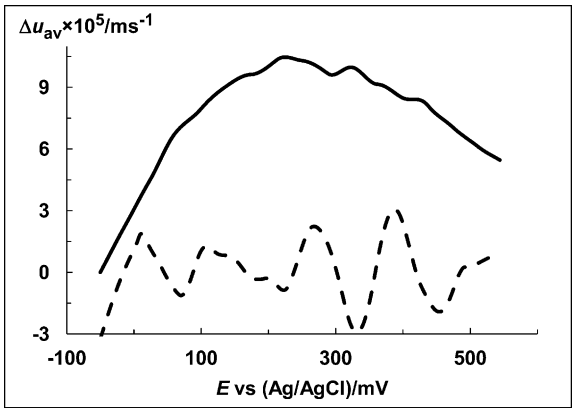

Figure 3. LOESS fit (solid line, sampling proportion and polynomial degree equal to 0.4 and 1, respectively) for change of average velocity of flow past gold coated sphere vs potential of sphere in 0.01 M $NaClO_4$ aqueous solution and LOESS fit (dashed line, sampling proportion and polynomial degree equal to 0.2 and 1, respectively) for residuals of average flow velocity, $u_{av}^{E=100\,\mathrm{mV}} = 0.17581$ m/s, three potential cycles at dE/dt=0.5 mV/s, (33625 flow velocity values), temperature from 26.0 to 26.4^{o}C.

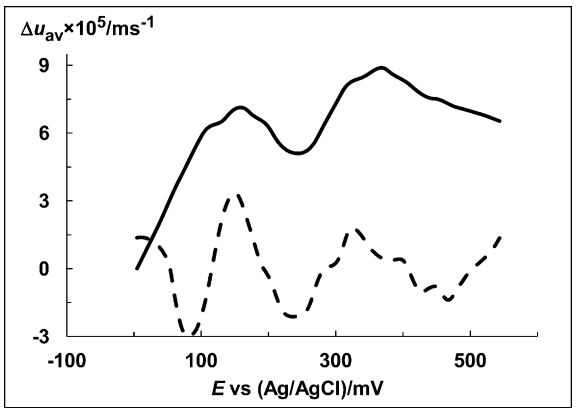

Figure 4. LOESS fit (solid line, sampling proportion and polynomial degree equal to 0.4 and 1, respectively) for change of average velocity of flow past gold coated sphere vs potential of sphere in 0.01 M NaCl aqueous solution and LOESS fit (dashed line, sampling proportion and polynomial degree equal to 0.2 and 1, respectively) for residuals of average flow velocity, $u_{av}^{E=0\,\mathrm{mV}} = 0.16852$ m/s, three potential cycles at dE/dt=0.5 mV/s, (31690 flow velocity values), temperature from 25.4 to 25.9^{o}C.

To gain better insight in goodness of LOESS fit (Fig. 2A, solid line), the residuals of this fit (Fig. 2B) were smoothed as a function of potential by using again the LOESS smoothing technique. To highlight the trends in residuals, the smaller sampling proportion (0.2) was used. The trends, which can be observed in LOESS fit for residuals (Fig. 2A, dashed line), do not considerably change the main features of the LOESS fit shown in the same figure.

The similar measurements of the flow velocity during polarisation of gold coated sphere were also performed in perchlorate and chloride solutions. In these measurements, the velocity sampling frequency was increased by detecting time for each 25 ml of liquid passed in addition to detecting time for each solution litre passed. Their LOESS fits against the potential are shown in Figs. 3 and 4 as solid lines.

The scatters of the residuals of LOESS fits (Figs. 3 and 4, solid lines) are not shown as they are similar to that shown in Fig. 2B. Only their LOESS fits (sampling proportion 0.2) are shown as dashed lines in Figs. 2 and 4. Again, it can be concluded that the trends of these LOESS fits for residuals do not considerably change the main features of the flow velocity LOESS fits for flow velocities shown in the same figures.

Adsorbing properties of used anions become stronger in the row $PF_6^- < ClO_4^- < Cl^-$. Hexafluorophosphate and perchlorate weakly adsorb on gold surface in water solutions. Their adsorption on gold surface becomes more significant at potentials more positive than +500 mV and +230 mV, respectively [1, 2]. In the less positive potential range, potential dependences of interfacial viscosity calculated from measured drag force data were compared with those obtained by using dual-resonator technique, which becomes unreliable when there are changes of electrode mass loading due to adsorption of solution species [1-2]. For this reason, dual-resonator technique does not produce reliable data on interfacial viscosity in the solution of chloride as it specifically adsorbs on gold surface. Comparison of earlier reported potential dependences of drag force [1, 2] with potential dependences of flow velocity (Figs. 2-4) reveals correlation between the main features of these dependences. In flow velocity change with potential (Figs. 2-4), the maxima are observed. For hexafluorophosphate solution, maximum is approximately at +140 mV (Fig. 2), what is close to the position of a minimum of drag force on a gold coated sphere in the same solution (+120 mV) [1]. For perchlorate solution, drag force minima are observed at +135 and +303 mV [2], whereas flow velocity maximum is between these potentials (Fig. 3) at +230 mV. For chloride solution, drag force minima are observed at +125 and +460 mV [2], whereas flow velocity maxima are at +150 and +380 mV (Fig. 3). It can be concluded that there is an approximate agreement between the potentials of flow velocity maxima and drag force minima. Discrepancies could be attributed to the errors of flow velocity measurements.

3.2. Effect of surface electric polarisation on the flow velocity near the surface and the interfacial viscosity

The maximum increase of flow velocity is ~0.05% of average velocity value (Figs. 2-4). Small increase of velocity seems to be in contradiction with earlier found rather significant change of drag

force and solution interfacial viscosity with potential change [1, 2]. However, it should not be of surprise because the area of the electrically polarized surface (sphere surface), where the decrease of interfacial viscosity of flowing solution can occur [1, 2], is rather small is in comparison with the area of inner surface of the tube (2 in Fig.1). The measured flow velocity is the average velocity of the flow through the tube. During positive polarization decrease of viscosity with potential occurs within the thin solution layer at the sphere surface and it is reasonable to conclude that increase of flow velocity is most pronounced in this solution region. This local increase of velocity should be much higher than the average flow velocity.

For further discussion, it should be remembered that drag forces on a sphere come primarily from viscous shearing stresses (skin friction) and differences in pressure. The net drag force F_{D} on a sphere could be divided into frictional drag F_{Df} and pressure drag F_{Dp} [4]:

$$C_{\mathrm{D}} = \frac{F_{\mathrm{D}}}{(1/2)\rho u_{\infty}^{2} A} = \frac{F_{\mathrm{Df}}}{(1/2)\rho u_{\infty}^{2} A} + \frac{F_{\mathrm{Dp}}}{(1/2)\rho u_{\infty}^{2} A} = C_{\mathrm{Df}} + C_{\mathrm{Dp}} \tag{4}$$

Decomposition (4) is based on an assumption that the pressure drag depends mostly on the shape of the body, while the friction drag depends essentially on the size of the surface of the body and not on the shape of the surface. However, the friction drag also depends on the shape of the surface, so that this decomposition is only approximately valid

The skin friction is the integral of the local wall shear stresses τ_w taken over the surface of the body. Correspondingly, skin-friction drag coefficient C_{Df} can be defined as the integral of local skin-friction coefficients C_{f} taken over the surface of the body. The relationship between C_{f} and τ_w is [7]

$$C_{\mathrm{f}} = \frac{\tau_w}{(1/2)\rho u_{\infty}^{2}} = \frac{\eta(\partial u/\partial y)_{y=0}}{(1/2)\rho u_{\infty}^{2}} \tag{5}$$

where u is the streamwise fluid velocity.

The pressure drag originates from the uneven pressure distribution on the body surface. The integral of the local pressure (modified by friction) taken over the surface of the body produces a pressure drag. The local pressure coefficient C_{p} is [7]

$$C_{\mathrm{p}} = \frac{p - p_{\infty}}{(1/2)\rho u_{\infty}^{2}} \tag{6}$$

where p is a pressure at the surface point at which pressure coefficient is being evaluated, p_{∞} is a pressure in the free stream, i.e. remote from any disturbance.

Although viscosity explicitly appears only in the expression of skin friction coefficient (5), decrease of viscosity at the surface can result in a decrease of an adverse pressure gradient. That delays both the flow detachment from the bonding surface and the formation of vortices on the downstream side of the sphere. Such effect results in decreased drag, particularly pressure drag, which is caused by the pressure differential between the front and rear surfaces of the sphere at the flow past a sphere. These considerations lead to the conclusion that earlier obtained decrease in interfacial viscosity [1, 2], calculated from the drag coefficient change with potential as described in section 1, is to some extent overestimated. Such conclusion also implies that an increase of flow velocity appears not only due to

the decrease of skin friction but of pressure differential as well. However, it is not possible to correct interfacial viscosity calculations as there is no quantitative theory for sphere drag in turbulent flow.

3.3. Potentiality of the use of wall electric polarization as a flow stability modifier for wall-bounded water flow

In wall-bounded flows, the small change of interfacial water properties such as viscosity and density may have crucial effect on the fluid flow field. It follows from the instantaneous streamwise (x direction) momentum equation, which at the non-moving and impermeable wall of small curvature (y=0, where y is the normal to the wall surface) reads [8]:

$$\rho_w \partial u/\partial t\big|_{y=0} + \partial p/\partial x\big|_{y=0} - \partial \eta/\partial y\big|_{y=0}\, \partial u/\partial y\big|_{y=0} = \eta \partial^2 u/\partial y^2\big|_{y=0} \qquad (7)$$

where ρ_w is the fluid density at the wall and t is the time. Equation (7) is valid for a fluid with variable density and viscosity. The second derivative of the velocity profile on the right-hand side of Eq. (7) represents the flux of vorticity, as shown by Lighthill [9]. The terms on the left-hand side of Eq. (7) can affect the sign of the second derivative of the velocity profile, i.e. the direction of the vorticity flux. Favourable pressure gradient ($\partial p/\partial x < 0$) or lower wall viscosity ($\partial \eta/\partial x > 0$) will cause the curvature of the velocity profile at the wall to become more negative what increases the lower critical Reynolds number and reduces amplification rates of unstable waves and, hence, increases the flow stability and its resistance to boundary-layer separation. Techniques, which do that, are termed as stability modifiers. It should be noted, however, that lowering the liquid viscosity near the surface results in an increase in the skin friction over the unmodified Blasius layer. Then it is necessary to keep the penalty below the saving: the net drag should be above that of the flat-plate laminar boundary layer but well below the viscous drag in the flat-plate turbulent flow. That can be achieved for flows with Reynolds numbers below 4×10^7 [8].

To the best of our knowledge, wall electrical polarization has not been considered as a flow stability modifier, although it has been reported that by controlling the applied potential, it is possible to control the viscosity liquid layer close to the solid interface [10]. In addition, this effect has been put to the test in a hydroelectric power plant what has shown the decrease of head loss over the length of the turbine pipe [11]. It should be noted that the Reynolds number of the turbine pipe flow was 5×10^6 what was well below the upper limit 4×10^7. It seems reasonable to assume that wall electrical polarization can be considered as a flow stability modifier for wall-bounded flow because it evidently increases the flow stability and its resistance to boundary-layer separation.

4. CONCLUSION

The measured potential dependences of the velocity of the flow of aqueous solutions past the gold coated spheres correlate with earlier reported potential dependences of drag force on these spheres [1, 2]. Flow velocity maxima (~0.05% of average velocity) are observed near the potentials of drag force minima. Small increase of velocity is not in contradiction with earlier found rather significant change of drag force the sphere. It is reasonable to conclude that the increase of flow velocity is most

pronounced within the thin solution layer at the sphere surface. This local increase of velocity should be much higher than the measured average velocity of the flow through the tube.

Earlier reported decrease in interfacial viscosity during positive potential scan [1, 2], which has been calculated from measured drag force via empirical relationship between drag force coefficient and dynamic viscosity, should be considered as to some extent overestimated. The used relationship does not account for interdependence of frictional and pressure drags. However, it is not possible to correct interfacial viscosity calculations as there is no quantitative theory for sphere drag in turbulent flow. For this reason, the decrease of interfacial viscosity by ~0.5 % at minimum, obtained by using piezoelectric resonator method [1, 2], should be considered as more reliable.

The results of present work, which have been obtained in the absence of confinement of fluid between a probe and surface, supplement published atomic force microscopy data by technological promise. In atomic force microscope and interfacial force microscope measurements, it has been shown that a surface can induce a drastic change of the effective viscosity of water in its close proximity [12-14], what can be controlled by applying the potential [10]. Our results show that the changes of interfacial layer properties, induced by applied potential, extend beyond the interface and can result in the bulk effects such as the change of wall-bounded flow velocity.

References

1. D. Plausinaitis, A.Pulmanas, M. Waskaas, R. Raudonis and V. Daujotis, *Electrochim. Acta*, 109 (2013) 756.
2. D. Plausinaitis, A. Pulmanas, V. Kubilius, R. Raudonis and V. Daujotis, *Electrochim. Acta*, 121 (2014) 278.
3. F.N. White, *Fluid Mechanics*, 4th ed., McGraw–Hill, Boston–Toronto (2002).
4. R. Clift, J.R. Grace and M.E. Weber, *Bubbles, Drops and Particles*, Academic Press, New York (1978).
5. E. Achenbach, *J. Fluid Mech*., 54 (1972) 565.
6. Reprinted from *Electrochim. Acta*, 109, D. Plausinaitis, A.Pulmanas, M. Waskaas, R. Raudonis and V. Daujotis, Piezoelectric resonator and drag force study of the properties of aninterfacial hexafluorophosphate solution layer at gold electrode surface, Page No. 758, Copyright (2013), with permission from Elsevier.
7. H. Schlichting, *Boundary-Layer Theory*, 7th ed., McGraw-Hill; New York-Toronto (1979).
8. M. Gad-el-Hak, *Flow Control: Passive, Active, and Reactive Flow Management*, Cambridge University Press; New York (2006).
9. M. J. Lighthill, *Introduction: Boundary Layer Theory*, in L. Rosenhead (Ed.), *Laminar Boundary Theory*, Oxford University Press, Oxford (1963) pp. 46-113.
10. S. Guriyanova, V.G. Mairanovsky and E. Bonaccurso, *J. Colloid Interface Sci.*, 360 (2011) 800.
11. M. Waskaas, V. Daujotis, K. E. Wolden, R. Raudonis and D. Plausinaitis, *Russ. J. Electrochem.*, 44 (2008) 602.
12. M. P. Goertz, J. E. Houston and X.-Y. Zhu, *Langmuir, 23* (2007) 5491.
13. T.-D. Li, J. Gao, R. Szoszkiewicz, U. Landman, E. Riedo, Phys. Rev. B, 75 (2007) 115415.
14. D. Ortiz-Young, H.-C. Chiu, S. Kim, K. Voitchovsky and E. Riedo, Nat. Commun., 4 (2013) 2482.